Published in final edited form as:
Magn Reson Med. 2009 August ; 62(2): 520–526. doi:10.1002/mrm.22034.

Incidental Magnetization Transfer Contrast by Fat Saturation Preparation Pulses in Multi-slice Look-Locker Echo Planar Imaging: Modulation of Signal Intensity and Bias on T_1 Measurement

Wanyong Shin[1], **Hong Gu**[1], and **Yihong Yang**[1]

[1] Neuroimaging Research Branch, National Institute on Drug Abuse, National Institutes of Health, Baltimore, MD 21224

Abstract

In this study, it is demonstrated that fat saturation (FS) preparation (prep) pulses generate incidental magnetization transfer contrast (MTC) in multi-slice Look-Locker imaging. It is shown that frequency-selective FS prep pulses can invoke MTC through the exchange between free and motion-restricted protons. Simulation reveals that the fractional signal loss by these MTC effects is more severe for smaller flip angles, shorter repetition times, and greater number of slices. These incidental MTC effects result in a signal attenuation at a steady state (up to 30%) and a T_1 measurement bias (up to 20%) when using inversion recovery Look-Locker EPI sequences. Furthermore, it is shown that water-selective MR imaging using binominal pulses has the potential to minimize the signal attenuation and provide unbiased T_1 measurement without fat artifacts in MR images.

Keywords

magnetic resonance imaging; magnetization transfer contrast; fat saturation pulse; Look-Locker EPI; T_1 measurement

Introduction

Magnetization transfer contrast (MTC) based on the exchange between highly mobile protons (^1H_f) and macromolecular protons (^1H_r) in biological tissues was first demonstrated by Wolff and Balaban (1). The underlying biophysical mechanism of magnetization transfer (MT) has been investigated extensively using theoretical modeling (2,3) and *in vivo* experiments (4,5). MTC effects can be achieved by employing continuous (1) or pulsed (6) off-resonance radiofrequency (RF) irradiation in imaging sequences.

Interestingly, incidental MTC has been reported primarily in multi-slice imaging sequences (7), in which the off-resonance excitation of slice-selective pulses induces unwanted MTC, leading to a loss of signal intensity. This phenomenon has been observed predominantly in multi-slice fast spin-echo (FSE) (8,9) and steady-state free precession (SSFP) (10) sequences, with increased MTC when a greater number of slices were acquired (7). It is intuitive that MTC is dependent on the number of off-resonance RF pulses applied per unit

Corresponding: Wanyong Shin or Yihong Yang, Neuroimaging Research Branch, National Institute on Drug Abuse, National Institutes of Health, 251 Bayview Blvd, Suite 200, Baltimore, MD, 21224, Phone: 443-740-2621 or 443-740-2621, Fax: 443-740-2734, shinwa@nida.nih.gov or yihongyang@intra.nida.nih.gov.

time and the power of these pulses to irradiate the ^1H_r pool. The former is related directly to the number of slices, while the latter is dependent on the flip angle (FA) and frequency offset of these pulses. When the off-resonance RF pulses have a relatively large FA (90° and 180° in FSE) and/or are repeated rapidly (SSFP), MTC is not negligible and the effects accumulate when the number of slices is increased.

Recently, in a measurement of the longitudinal relaxation time (T_1) of the brain using a multi-slice inversion-recovery Look-Locker echo-planar imaging (IR LL-EPI) sequence (11), we observed a significant signal loss at steady state and a change in the recovery rate during the inversion recovery procedure, when using fat saturation (FS) preparation (prep) pulses (see Fig.1). This phenomenon was prominent in gray and white matter, but not in cerebrospinal fluid (CSF). It was therefore suspected that the FS prep pulses, which were frequency-selective, generated MTC. This incidental and undesirable MTC by FS prep pulses is problematic, especially in quantitative MR measurements, such as T_1 measurements.

In this study, we systematically investigate the MTC effects by FS prep pulses in multi-slice IR LL-EPI sequences. Attenuation of signal intensity and T_1 measurement bias in the brain due to the FS prep pulses are demonstrated. Computer simulations, based on a two-pool exchange model, are performed to examine their dependence on imaging parameters such as the number of slices (SN), FA and repetition time (TR). The potential direct saturation of ^1H_f by FS prep pulses (bleed-over) is also investigated. As a solution to the problem, water-only excitation (WE) pulses, which generate frequency-selective excitation of water protons in the ^1H_f pool, show great potential to minimize the signal attenuation and T_1 measurement error, while avoiding chemical-shift artifacts from fat tissue.

Methods

MR experiments

Studies were performed under a protocol approved by the Institutional Review Board at the National Institute on Drug Abuse; all subjects provided written informed consent. Three healthy subjects (32±12 years, 2 females) were scanned on a Siemens 3T Allegra scanner (Siemens Medical Solutions, Erlangen, Germany) using a quadrature volume coil. To measure a reference T_1, an IR-EPI sequence was used to collect data on a single brain slice, using a non-selective inversion with 10 different inversion times (TIs), respectively, ranging from 34 ms to 15000 ms. The other imaging parameters were: TR/TE = 30s/14ms, FA=16°, FOV=220×220 mm^2, matrix=64×64, and slice thickness=5mm. To minimize potential effects from instrumental instabilities and temperature fluctuations due to repeated RF pulses and gradients, the baseline T_1 measurement was performed twice before and after IR LL-EPI scans (described below) and averaged.

IR LL-EPI scans with a varying number of slices (SN = 1, 3, 5, 7, and 9) were performed on the subjects. Two IR LL-EPI sequences with different strategies to suppress the fat signal were used: 1) FS prep pulse (FS); IR LL-EPI with a frequency-selective FS prep pulse (on the fat resonance) followed by gradient crushers and then a slice-selective excitation pulse, and 2) water-only excitation pulses (WE); IR LL-EPI with WE pulses consisting of composite binominal pulses to generate a slice-selective excitation of the free water resonance (12,13). The FS prep pulse was based on a Gaussian function with duration of 5112 μs. The WE pulses were “1-2-1” binominal pulses (12,13) used to excite the free water molecules. For comparison, IR LL-EPI scans with a conventional water excitation pulse but without any FS prep pulses (noFS) were also performed. The center slice in IR LL-EPI scans was aligned to that in the IR-EPI, and compared across different scans. To minimize the T_1 measurement bias due to imperfect excitation pulses, optimal imaging parameters for

the IR LL-EPI sequences were used based on previous studies (14): FA=16°, TR/TE = 400/14ms, 25 time sampling points during an IR period of 10 s. T_1 values were calculated from the recovery of the signal intensity:

$$1/T_1^* = 1/T_1 - \log(\cos\theta)/TR, \quad [1]$$

where T_1^* is the apparent longitudinal magnetization relaxation time obtained from LL sequences (14,15). T_1 and the longitudinal magnetization at steady state, M_{SS} values were measured in white matter (WM) and gray matter (GM) regions of interest (ROIs), which were chosen based on a full-width-at-half-maximum (FWHM) method to fit two Gaussian distributions from the measured T_1 distribution in the IR-EPI image (16). Relative T_1 (rel.T_1) and relative M_{SS} (rel.M_{ss}) were defined as measured T_1 and M_{SS} from the IR LL-EPI sequences with FS or WE, divided by T_1 and M_{SS} from the IR-LL-EPI sequence without FS (noFS), respectively.

MTC and bleed-over effects (S_f and S_r measurements)

Mathematical modeling was designed to analyze the signal saturation and the relaxation rate change induced by FS prep pulses in multi-slice MR sequences. A two-pool exchange model describing pulsed MTC by Pike (17) was adapted and modified (See Appendix). Pike's analytic model introduced the fractional saturation in the ^1H_f compartment (S_f) and the fractional saturation in the ^1H_r compartment (S_r) by off-resonance pulses. In this study, S_f and S_r by FS prep pulse were considered. Potential bleed-over effects by FS were also investigated. From the simulated and experimental data, S_r and S_f in WM and GM were estimated by minimizing the sum of squared error (SSE) across the number of slices, defined as the difference between the mathematical model and the experimental data:

$$SSE(S_f, S_r) = \sum_{SN} \left(rel.M_{ss}(S_f, S_r, SN) - rel.M_{ss}(SN) \right)^2, \quad [3]$$

where rel.M_{SS} (S_f, S_r, SN) is calculated from Eqn. [A-21]

Dependency of imaging parameters on MTC by FS

Simulations were performed to examine the relationship between the MTC effects and the imaging parameters. MTC effects which induced signal attenuation and T_1 bias were assessed as a function of SN, TR and FA. Simulated data were generated with various SN (1, 3, 5, 7 and 9), TR (0.4, 0.8 1.2, 1.6 and 2 s), and FA (16°, 32°, 48°, 64°, and 80°) values, respectively. The intrinsic parameters for GM ($T_{1,f}$ = 1.15s, $T_{1,r}$ = 1.2s, k_f =4 Hz and F=0.07) adapted from the literature (18) were used in the simulations.

Results

Signal intensity and T_1 measurement

Fig.2 and Tab.1 show the relative T_1 and M_{SS} of representative ROIs in WM and GM from the three subjects as a function of SN. For comparison, data from a phantom filled with distilled water are also shown. With FS prep pulses, signal loss in the WM and GM ROIs was more severe as the SN was increased (Fig.2a); a similar tendency was observed in the measured T_1 values (Fig.2b). However, signal intensity and measured T_1 in the water phantom did not change significantly with SN. FS prep pulses caused approximately 30%

signal loss and 20% T_1 underestimation in WM and GM when SN was 9. In contrast, IR LL-EPI sequence with WE pulses did not show attenuation of signal intensity or T_1 measurement bias (Fig.2c and 2d).

MTC and bleed-over effects

S_r and S_f values were estimated to be 0.802 and 0.997 in WM, and 0.806 and 0.998 in GM, respectively. Based on the two-pool exchange model (see Appendix), if the MTC effects are neglected (S_r=1 and S_f=0.998) the rel.M_{SS} is expected to be 0.959, which is inconsistent with the experimental results. However, if the bleed-over effects are neglected (S_r=0.806 and S_f=1) the rel.M_{SS} is calculated as 0.776, which is close to the experimental data (0.751). These results indicate that MTC effects are largely responsible for the signal attenuation and T_1 bias in multi-slice LL-EPI sequences.

Dependence of MTC effects on image parameters

The dependence of the fractional signal loss on image parameters (FA, TR and SN) with a FS prep pulse was evaluated with measured S_r (0.806) and S_f (0.998) values in GM. Fig.3 shows that the signal attenuation is more severe as FA decreases, TR shortens and SN increases. Similar results were obtained using S_r and S_f values measured in WM.

Comparison of T_1 maps

Fig.4 shows the representative T_1 maps obtained from the conventional IR-EPI sequence (Fig.4a) and the corresponding center slice T_1 maps from three IR LL-EPI sequences with different preparation and excitation pulses: without FS (noFS) (Fig.4b), with FS (Fig.4c), and with WE (Fig.4d). Compared to the conventional IR-EPI sequence (as a “gold standard”), T_1 values from IR LL-EPI with FS were underestimated (Fig.4c), while the values from IR LL-EPI with WE were consistent (Fig.4d). The T_1 map from the IR LL-EPI sequence without FS shows a “ringing” artifact (arrow) due to a chemical shift of the fat signal.

Voxel-wise comparisons of the T_1 values from the IR-EPI sequence and the center slice of each IR LL-EPI scan from the three subjects are plotted in Fig.5. Spatial smoothing with a Gaussian filter (6 mm FWHM) was performed to minimize head motion effects and image distortion between scans. Voxels with T_1 values larger than 2.5 s were excluded for the comparison. The T_1 values from IR LL-EPI with FS were underestimated by approximately 17.7±4.0%. The error was substantially reduced in data acquired from IR LL-EPI without FS (4.3±6.6%) and with WE (5.6±4.1%). In addition, the precision was considerably improved in data from IR LL-EPI with WE compared to that from IR LL-EPI without FS, as indicated by significantly smaller standard deviations, probably due to their differences in effective fat signal suppression.

Discussion

Frequency-selective FS pulses have been widely used in EPI-based sequences to suppress unwanted fat signal. The off-resonance irradiation (relative to ^1H_f) may induce non-negligible MTC effects and result in attenuation of the ^1H_f signal. In this study, we investigated this phenomenon in multi-slice LL-EPI sequences and assessed its effects on the accuracy of T_1 measurement. Our results showed that the FS prep pulses can result in a maximum of 30% signal loss at steady state and a 20% error in T_1 quantification. Multi-slice imaging techniques have been widely used to acquire images covering the entire brain. However, the number of FS pulses per unit time usually increases when a larger number of slices are collected in multi-slice imaging, resulting in more severe signal attenuation as shown in Fig.2a. These MTC effects can lead to considerable errors in quantitative MRI

techniques, such as T_1 measurement using LL acquisition (Fig.2b). The signal loss is also dependent on imaging parameters such as FA and TR (Fig.3). Since the T_1 measurement using Look-Locker sequences performs better with a relatively low FA and a small TR to better observe signal recovery (14), these sequences are particularly vulnerable to MTC-induced errors in quantification.

Binomial composite pulses have been frequently used to selectively irradiate spins in a specific frequency range. The basic principle of binominal WE pulses is to excite water protons at a full strength and to suppress fat protons by setting the first null frequency to the fat resonance. If the RF pulse is a delta function, the "1-2-1" composite RF pulses follow a cosine function over the frequency domain. Assuming 434 Hz between water and fat resonance frequencies at 3T, the 1-2-1 WE pulses have a 434 Hz FWHM. A conventional water-excitation RF pulse typically has a larger bandwidth than WE pulses, covering the fat resonance frequency. The narrower bandwidth of the WE pulses might explain the observation that M_{SS} values with WE pulses are slightly lower than those without FS in Fig. 2 and Tab.1 (rel. M_{SS} = 98.6% in WM, 97.5% in GM, and 97.4% in water, respectively). Nevertheless, we demonstrated in this study that spatial-spectral selective RF pulses with a narrow bandwidth provided great potential to minimize the MTC effects and chemical shift artifacts.

Voxel-wise T_1 comparisons in Fig.5 showed that IR LL-EPI without FS and with WE overestimated T_1 by 4.3% and 5.6%, respectively, compared with the baseline measurement. For an accurate T_1 measurement using LL approaches it is known that B1 inhomogeneity is the one of the main error sources (19). Recent studies demonstrated that the accuracy of T_1 measurements depend on the applied flip angle, RF excitation efficiency (γ), T_1 and TR, formulated as $T_1 \ln(\cos\alpha / \cos\gamma\alpha) / TR$ (14). Note that γ is the ratio of the actual FA to the ideal FA, which depends on spatial location. The overall B_1 inhomogeneity in the human brain is approximately 0.9 based on previous studies (20). Therefore, a 4.3% T_1 overestimation when using IR LL-EPI without FS can be explained by imperfect RF excitation efficiency, and the 5.6% T_1 overestimation observed in the LL method with WE pulses might be caused by a further reduction in efficiency due to the narrow WE pulse bandwidth.

The FS prep pulse used in this study was set to the default setting in Siemens 3T scanners (duration of 5120 μs, bandwidth of 275 Hz, FA of 110°). Although these parameters are commonly used for FS pulses, parameter changes may result in different levels of signal attenuation and T_1 measurement bias even when other experimental conditions are kept the same (21). The fractional saturation indices, S_r and S_f, may also be dependent on the FS pulse parameters. Optimization of the FS prep pulse to generate less MTC effects while efficiently minimizing the fat-induced artifacts would be useful for future studies.

The potential MTC effects by off-resonance irradiation from the water excitation RF pulses applied on other slices were not investigated in this study. We used a relatively small FA (16°) so that the MTC from these off-resonance irradiations was expected to be very small for the following reasons. First, the irradiation of the ^1H_r pool by the small FA pulses could be ignorable ($\cos 16° = 0.96$). Second, assuming a slice thickness of 5 mm and a slice-selective gradient of 10mT/m, the frequency difference between the adjacent slices was larger than 20 kHz, at which the MTC effects attenuated significantly. Third, the frequency difference increased as the excited slice was farther away from the slice of interest, so that MTC might not accumulate in multi-slice imaging. However, RF pulses with a relative large FA (>60°) in EPI acquisitions might invoke non-negligible MTC by the off-resonance irradiation of the water excitation RF pulses applied to other imaging planes. These MTC effects may be avoided completely by using 3-dimensional imaging acquisition strategies.

Conclusions

In this study, we demonstrated that FS prep pulses could invoke incidental MTC effects in multi-slice imaging sequences, resulting in significant attenuation of signal intensity due to dynamic exchange between the ^1H_f and ^1H_r pools. These incidental MTC effects would generally have a detrimental impact on quantitative MRI techniques. In particular, we demonstrated the influence of the MTC effects on T_1 measurements using an IR LL-EPI sequence with a FS prep pulse. The dependence of these MTC effects on imaging parameters (FA, TR and SN) was assessed using simulation, showing that the effects were more severe when a smaller FA value, shorter TR, or larger SN was used. We further showed that WE pulses had the potential to minimize the signal attenuation and T_1 measurement error, while suppressing fat artifacts in MR images.

Acknowledgments

This work was supported by the Intramural Research Program of the National Institute on Drug Abuse (NIDA), National Institutes of Health (NIH). The authors would like to thank Dr. Thomas Ross and Dr. Yufen Chen for helpful discussions.

Appendix

A two-pool analytic description of signal evolution in the presence of exchange between the ^1H_f and ^1H_r pools has been proposed in previous studies (6). The longitudinal magnetization change between the ^1H_f and ^1H_r pools can be described by two first-order exchange rate constants: k_f (from ^1H_f to ^1H_r) and k_r (from ^1H_r to ^1H_f). Without any irradiation from the applied RF pulses, longitudinal magnetization components in the ^1H_f pool ($M_{z,f}$) and the ^1H_r pool ($M_{z,r}$) can be described as

$$dM_{z,f}/dt = R_{1,f}\,(M_{0,f} - M_{z,f}) - k_f\,M_{z,f} + k_r\,M_{z,r} \quad [A\text{-}1]$$

$$dM_{z,r}/dt = R_{1,r}\,(M_{0,r} - M_{z,r}) - k_r\,M_{z,r} + k_f\,M_{z,f} \quad [A\text{-}2]$$

where $R_{1,f}$ and $R_{1,r}$ are the intrinsic longitudinal relaxation rates in the ^1H_f and ^1H_r pools, respectively. $M_{0,f}$ and $M_{0,r}$ represent the equilibrium longitudinal magnetization in the ^1H_f and ^1H_r pools, respectively. Considering only the longitudinal components in this model, $M_{z,f}$ and $M_{z,r}$ are simplified and replaced with M_f and M_r, respectively.

The solutions of these coupled equations can be expressed as bi-exponentials;

$$M_f = M_{0,f} + C_1 \exp(-\lambda_1 t) + C_2 \exp(-\lambda_2 t) \quad [A\text{-}3]$$

$$M_r = M_{0,r} + D_1 \exp(-\lambda_1 t) + D_2 \exp(-\lambda_2 t) \quad [A\text{-}4]$$

where

$$C_{1,2}=\left(\pm\left(R_{1,f}+k_f-\lambda_{2,1}\right)\left(M_f\left(t_0\right)-M_{0,f}\right)\mp k_r\left(M_r\left(t_0\right)-M_{0,r}\right)\right)/\left(\lambda_1-\lambda_2\right) \quad [A-5]$$

$$D_{1,2}=\left(\pm\left(R_{1,r}+k_r-\lambda_{2,1}\right)\left(M_r\left(t_0\right)-M_{0,r}\right)\mp k_f\left(M_f\left(t_0\right)-M_{0,f}\right)\right)/\left(\lambda_1-\lambda_2\right) \quad [A-6]$$

in which

$$\lambda_{1,2}=\left(R_{1,f}+k_f+R_{1,r}+k_r\right)/2\pm\sqrt{\left(R_{1,f}-R_{1,r}+k_f-k_r\right)^2+4k_r k_f}\,)/2 \quad [A-7]$$

To simplify the equations, it is assumed that 1) each FS pulse is applied instantaneously, 2) M_f is excited only by on-resonance slice-selective RF pulses, and partially saturated by the FS pulse, 3) M_r is partially saturated by FS, and 4) the transverse magnetization before the excitation is negligible due to the applied gradient spoilers.

To determine the longitudinal magnetization, M_n^- and M_n^+ are considered as before and after the excitation pulses in the nth slice. Using a column vector, $\overline{M}_z(=[M_f \;\; M_r]^T)$, the longitudinal magnetization in both the ^1H_f and ^1H_r pools can be tracked.

$$\overline{M}_1^+=\overline{S}_{on}\,\overline{M_1^-} \quad [A-8]$$

$$\overline{M}_n^+=\overline{S}_{off}\,\overline{M_n^-} \;\; (2\le n\le SN) \quad [A-9]$$

where $\overline{S}_{on}$ and $\overline{S}_{off}$ are diagonal matrices in on- and off-resonance excitation, respectively

$$\overline{S}_{on}=\left[\left[S_f\cos\alpha \quad 0\right]^T \quad [0 \quad S_r]^T\right] \quad [A-10]$$

$$\overline{S}_{off}=\left[[1 \quad 0]^T \quad [0 \quad S_r]^T\right] \quad [A-11]$$

where S_f and S_r are fractions in the H_f and H_r pools, respectively, irradiated (or saturated) by the FS pulse.

Using the matrix form of the general solution of Eqns.[A5-A9], the relaxation during the time interval between the acquisitions of two slices (TR / SN) can be written as;

$$\overline{M}_z(t=t_0+TR/SN)=\overline{AM}_z\left(t_0\right)+\overline{BM}_0 \quad [A-12]$$

where $\overline{M}_0=\begin{bmatrix} M_{0,f} & M_{0,r} \end{bmatrix}^T$. $\bar{A}$ and $\bar{B}$ are 2×2 matrices with elements $a_{i,j}$ and $b_{i,j}$, respectively. The elements of the matrices are expressed as follows:

$$a_{1,1}=((R_{1,f}+k_f-\lambda_2)E_1-(R_{1,f}+k_f-\lambda_1)E_2)/(\lambda_1-\lambda_2) \quad \text{[A-13]}$$

$$a_{1,2}=(k_r(E_2-E_1))/(\lambda_1-\lambda_2) \quad \text{[A-14]}$$

$$a_{2,1}=(k_f(E_2-E_1))/(\lambda_1-\lambda_2) \quad \text{[A-15]}$$

$$a_{2,2}=((R_{1,r}+k_r-\lambda_2)E_1-(R_{1,r}+k_r-\lambda_1)E_2)/(\lambda_1-\lambda_2) \quad \text{[A-16]}$$

$$b_{1,1}=(-(R_{1,f}+k_f-\lambda_2)E_1+(R_{1,f}+k_f-\lambda_1)E_2+\lambda_1-\lambda_2)/(\lambda_1-\lambda_2) \quad \text{[A-17]}$$

$$b_{1,2}=(k_r(E_1-E_2))/(\lambda_1-\lambda_2) \quad \text{[A-18]}$$

$$b_{2,1}=(k_f(E_1-E_2))/(\lambda_1-\lambda_2) \quad \text{[A-19]}$$

$$b_{2,2}=(-(R_{1,r}+k_r-\lambda_2)E_1+(R_{1,r}+k_r-\lambda_1)E_2+\lambda_1-\lambda_2)/(\lambda_1\backslash\lambda_2) \quad \text{[A-20]}$$

where $E_1 = \exp(-\lambda_1 TR/SN)$ and $E_2 = \exp(-\lambda_2 TR/SN)$

Combining the above equations, the longitudinal magnetization immediately after TR ($\overline{M}_{SN+1}$) can be expressed as

$$\overline{M}_{SN+1}=\left(\overline{AS}_{off}\right)^{SN-1}\left(\overline{AS}_{on}\right)\overline{M}_1+\left[\sum_{i=0}^{SN-1}\left(\overline{AS}_{off}\right)^i\right]\overline{BM}_0 \quad \text{[A-21]}$$

When the longitudinal magnetization approaches steady state, its intensity M_{SS} can be obtained by solving Eqn.[A-21],

$$\overline{M}_{SS}=\left[1-\left(\overline{AS}_{off}\right)^{SN-1}\left(\overline{AS}_{on}\right)\right]^{-1}\left[\sum_{i=0}^{SN-1}\left(\overline{AS}_{off}\right)^i\right]\overline{BM}_0 \quad \text{[A-22]}$$

References

1. Wolff SD, Balaban RS. Magnetization transfer contrast (MTC) and tissue water proton relaxation in vivo. Magn Reson Med. 1989; 10(1):135–144. [PubMed: 2547135]
2. Henkelman RM, Huang X, Xiang QS, Stanisz GJ, Swanson SD, Bronskill MJ. Quantitative interpretation of magnetization transfer. Magn Reson Med. 1993; 29(6):759–766. [PubMed: 8350718]
3. Graham SJ, Henkelman RM. Understanding pulsed magnetization transfer. J Magn Reson Imaging. 1997; 7(5):903–912. [PubMed: 9307918]
4. Kruiskamp MJ, de Graaf RA, van VG, Nicolay K. Magnetic coupling of creatine/phosphocreatine protons in rat skeletal muscle, as studied by (1)H-magnetization transfer MRS. Magn Reson Med. 1999; 42(4):665–672. [PubMed: 10502754]
5. Quesson B, Thiaudiere E, Delalande C, Dousset V, Chateil JF, Canioni P. Magnetization transfer imaging in vivo of the rat brain at 4.7 T: interpretation using a binary spin-bath model with a superLorentzian lineshape. Magn Reson Med. 1997; 38(6):974–980. [PubMed: 9402199]
6. Pike GB, Glover GH, Hu BS, Enzmann DR. Pulsed magnetization transfer spin-echo MR imaging. J Magn Reson Imaging. 1993; 3(3):531–539. [PubMed: 8324313]
7. Dixon WT, Engels H, Castillo M, Sardashti M. Incidental magnetization transfer contrast in standard multislice imaging. Magn Reson Imaging. 1990; 8(4):417–422. [PubMed: 2392030]
8. Melki PS, Mulkern RV. Magnetization transfer effects in multislice RARE sequences. Magn Reson Med. 1992; 24(1):189–195. [PubMed: 1556927]
9. Santyr GE. Magnetization transfer effects in multislice MR imaging. Magn Reson Imaging. 1993; 11(4):521–532. [PubMed: 8316065]
10. Bieri O, Scheffler K. On the origin of apparent low tissue signals in balanced SSFP. Magn Reson Med. 2006; 56(5):1067–1074. [PubMed: 17036284]
11. Look DC, Locker DR. Time saving in measurement of NMR and EPR relaxation times. Rev Sci Instrum. 1970; 41:250–251.
12. Schick F, Forster J, Machann J, Huppert P, Claussen CD. Highly selective water and fat imaging applying multislice sequences without sensitivity to B1 field inhomogeneities. Magn Reson Med. 1997; 38(2):269–274. [PubMed: 9256107]
13. Schick F. Simultaneous highly selective MR water and fat imaging using a simple new type of spectral-spatial excitation. Magn Reson Med. 1998; 40(2):194–202. [PubMed: 9702701]
14. Shin W, Gu H, Yang Y. Fast High-Resolution T_1 Mapping using Inversion-Recovery Look-Locker Echo-Planar Imaging at Steady State: Optimization for Accuracy and Reliability. Magn Reson Med. 2009 in press.
15. Crawley AP, Henkelman RM. A comparison of one-shot and recovery methods in T1 imaging. Magn Reson Med. 1988; 7(1):23–34. [PubMed: 3386519]
16. Shin W, Cashen TA, Horowitz SW, Sawlani R, Carroll TJ. Quantitative CBV measurement from static T1 changes in tissue and correction for intravascular water exchange. Magn Reson Med. 2006; 56(1):138–145. [PubMed: 16767742]
17. Pike GB. Pulsed magnetization transfer contrast in gradient echo imaging: a two-pool analytic description of signal response. Magn Reson Med. 1996; 36(1):95–103. [PubMed: 8795027]
18. Smith SA, Farrell JA, Jones CK, Reich DS, Calabresi PA, van Zijl PC. Pulsed magnetization transfer imaging with body coil transmission at 3 Tesla: feasibility and application. Magn Reson Med. 2006; 56(4):866–875. [PubMed: 16964602]
19. Wang J, Mao W, Qiu M, Smith MB, Constable RT. Factors influencing flip angle mapping in MRI: RF pulse shape, slice-select gradients, off-resonance excitation, and B0 inhomogeneities. Magn Reson Med. 2006; 56(2):463–468. [PubMed: 16773653]
20. Samson RS, Wheeler-Kingshott CA, Symms MR, Tozer DJ, Tofts PS. A simple correction for B1 field errors in magnetization transfer ratio measurements. Magn Reson Imaging. 2006; 24(3):255–263. [PubMed: 16563954]
21. Martirosian P, Boss A, Deimling M, Kiefer B, Schraml C, Schwenzer NF, Claussen CD, Schick F. Systematic variation of off-resonance prepulses for clinical magnetization transfer contrast imaging at 0.2, 1.5, and 3.0 tesla. Invest Radiol. 2008; 43(1):16–26. [PubMed: 18097273]

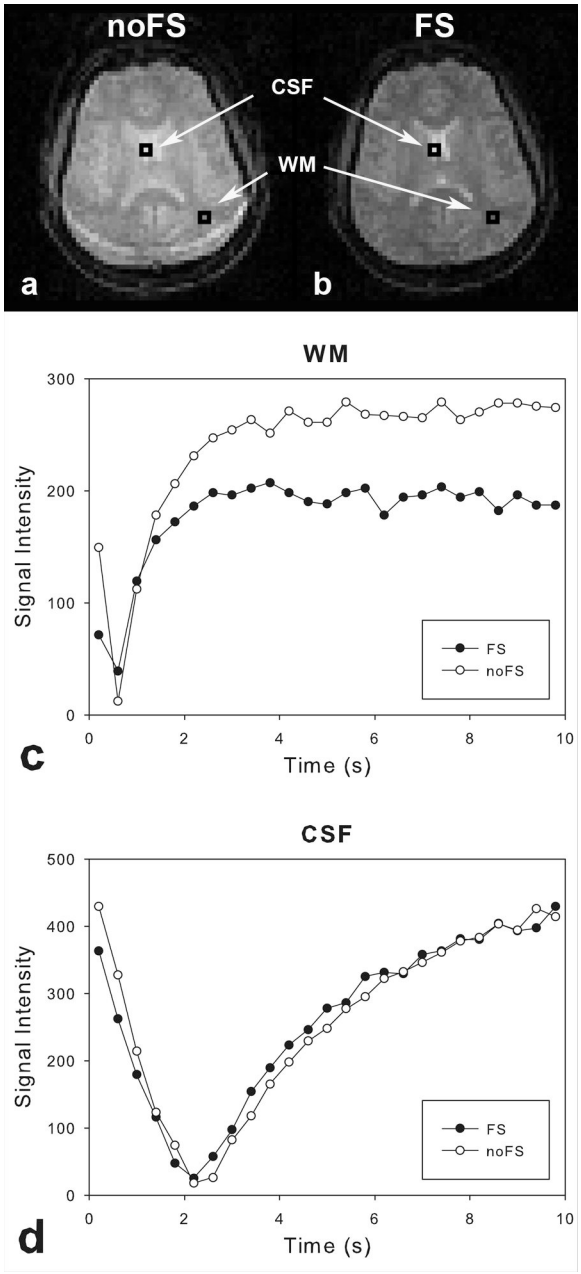

Fig 1.

A comparison of representative image intensities using IR LL-EPI with (a) and without (b) FS pulses. Other imaging parameters were identical in the two sequences. Two ROIs were chosen to represent WM and CSF, respectively. Black and white dots represent the signal regrowth from IR LL-EPI with and without FS prep pulses, respectively. Note that signals in WM (c) show differences in effective recovery time constant (T_1*) and intensity at steady state (M_{SS}) with and without FS prep pulses, while signals in CSF (d) have no significant difference.

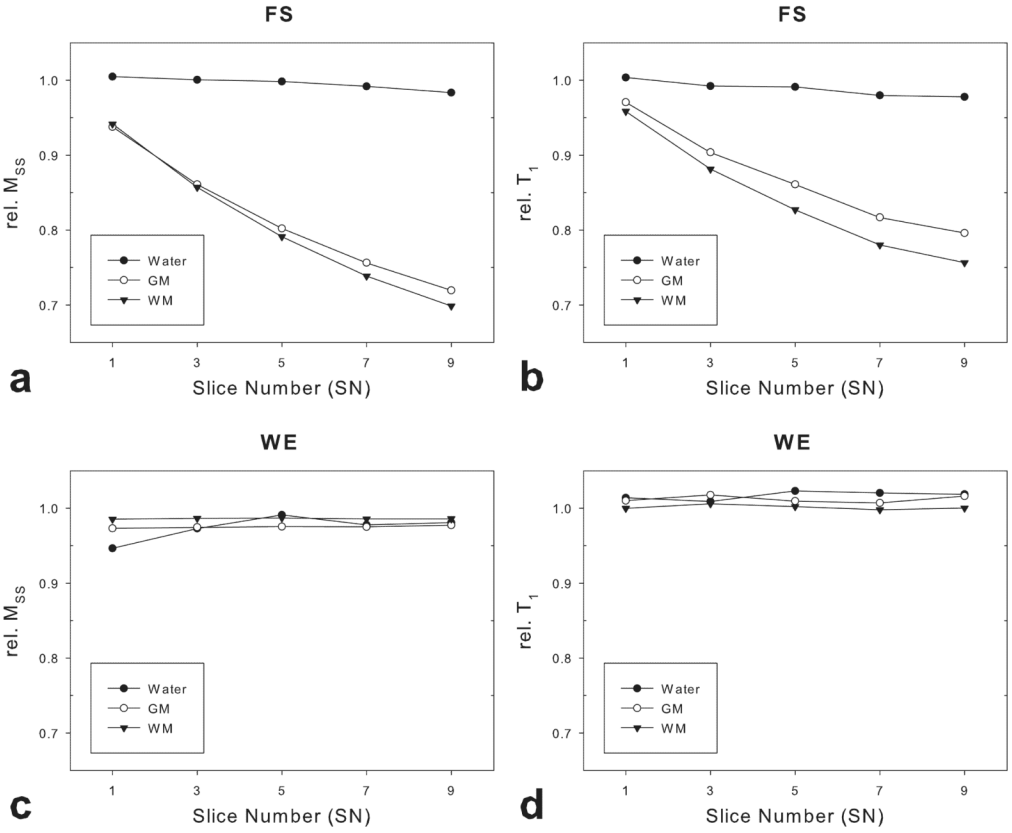

Fig 2.

The signal attenuation and T_1 measurement bias using IR LL-EPI as a function of the number of slices. Rel. M_{SS} and rel.T_1 values were compared in WM, GM and a distilled water phantom with FS prep and WE pulses, respectively.

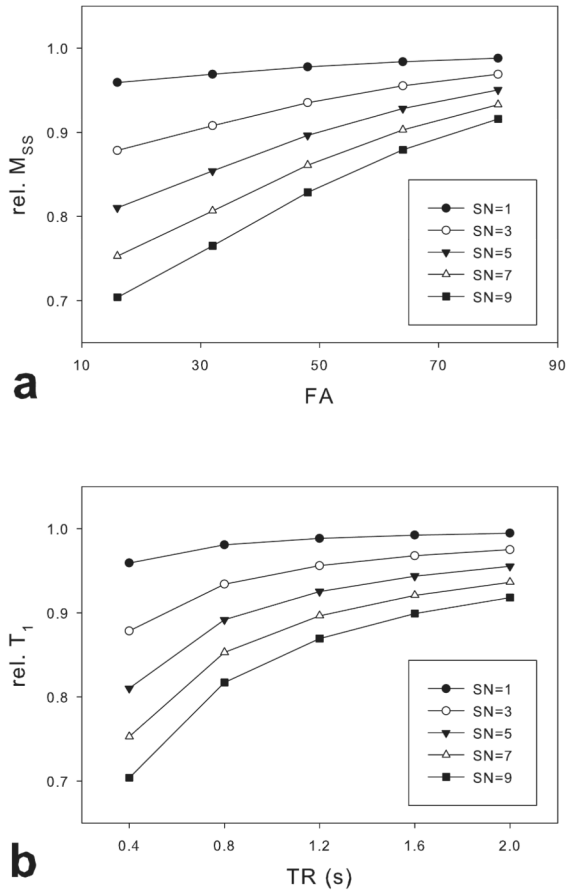

Fig 3.

The fractional signal loss as a function of FA or TR, simulated using the two-pool model described in the Appendix. The fractional signal loss, or rel. M_{SS} was simulated with varying FA and SN while TR was fixed (400ms) (a), and varying TR and SN while FA was fixed (16°) (b).

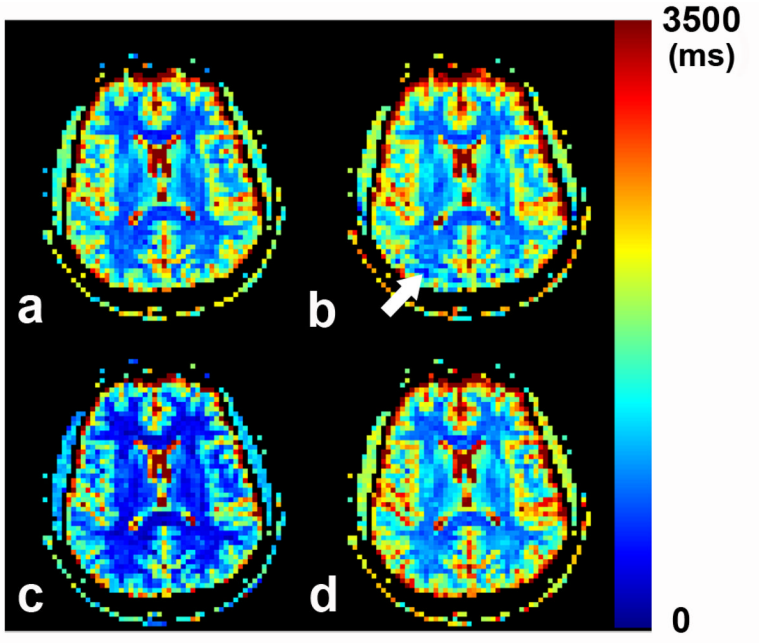

Fig 4.

A comparison of representative T_1 maps, obtained from conventional IR-EPI as a baseline (a), from IR LL-EPI without any prep pulse (b), from IR LL-EPI with a FS prep pulse (c), and from IR LL-EPI with WE pulses (d). The white arrow shows the “ringing” artifact due to chemical shift difference between fat and free water.

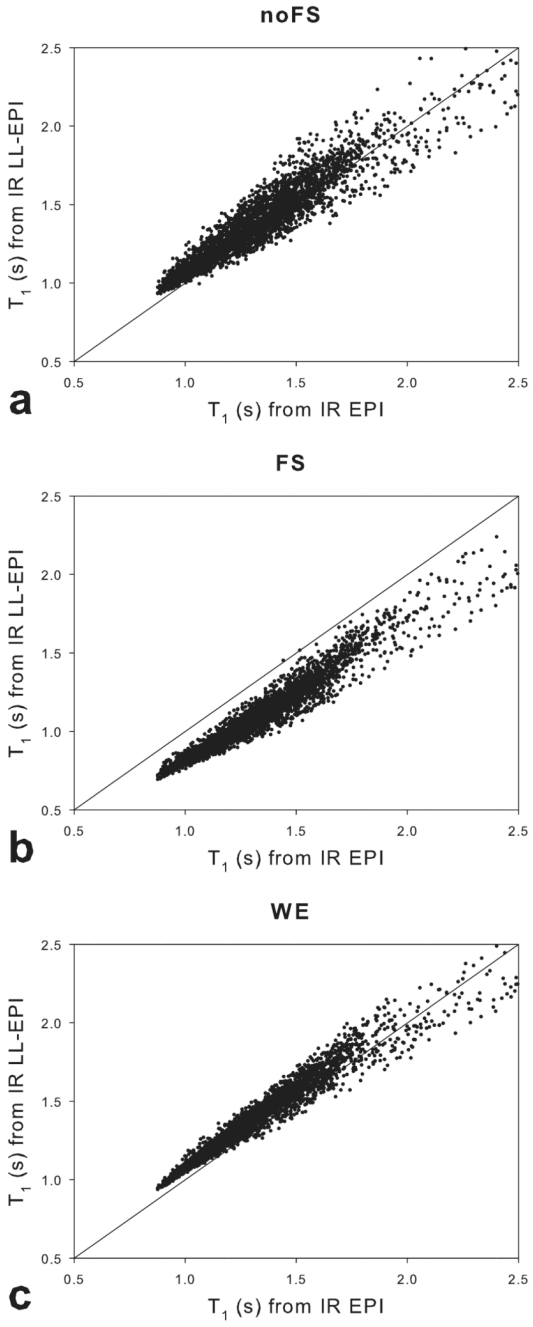

Fig 5.

A voxel-wise comparison of T_1 values in a slice of the brain. The x-axes represents the baseline T_1 values from IR-EPI, and the y-axes represent T_1 values from IR LL-EPI without any prep pulses (a), with a FS pre pulse (b), and with WE pulses (c). The dash line shows the identity relationship (y = x).

Tab. 1

	Prep. pulse	Tissue	SN				
			1	3	5	7	9
rel. M_{SS} (%)	FS	WM	94.2±0.6	85.7±0.3	79.1±0.4	73.8±0.6	69.9±0.5
		GM	93.8±0.5	86.1±0.5	80.2±0.4	75.6±0.7	72.0±0.9
	WE	WM	98.6±2.4	98.7±2.3	98.7±2.2	98.6±2.2	98.6±2.2
		GM	97.3±2.3	97.5±2.2	97.6±2.3	98.6±2.2	98.6±2.1
rel. T_1 (%)	FS	WM	95.9±1.1	88.2±1.2	82.7±1.5	78.0±1.8	75.7±2.3
		GM	97.1±0.8	90.4±1.2	86.1±0.8	81.7±0.9	79.6±0.8
	WE	WM	100.0±1.7	100.1±1.7	100.0±1.6	99.8±2.1	100.0±2.9
		GM	101.0±1.3	101.8±1.4	101.0±0.8	100.7±1.4	101.6±1.3